

Cerebellar astrocytic alterations in depression

Naguib Mechawar

naguib.mechawar@mcgill.ca

McGill University https://orcid.org/0000-0003-4960-756X

Christa Hercher Gina Abajian Maria Antonietta Davoli Gustavo Turecki

McGill University https://orcid.org/0000-0003-4075-2736

Article

Keywords:

Posted Date: September 25th, 2025

DOI: https://doi.org/10.21203/rs.3.rs-7593301/v1

License: © This work is licensed under a Creative Commons Attribution 4.0 International License.

Read Full License

Additional Declarations: The authors have declared there is NO conflict of interest to disclose

Abstract

Accumulating evidence suggests dysfunction of cerebellar-cerebral circuits in depression. However, the potential cellular and molecular alterations associated with depression in the cerebellum remain largely uncharacterized. While postmortem findings in the cerebral cortex indicate astrocyte dysregulation in depressed individuals who died by suicide (DS), the extent to which depression potentially alters cerebellar astrocytes is not well understood. In this study, two canonical astrocyte markers, glial fibrillary acidic protein (GFAP) and aldehyde Dehydrogenase-1 Family member L1 (ALDH1L1) were used to quantify cerebellar astrocyte subtypes, Bergmann glia (BG) in the Purkinje cell layer (PCL), velate astrocytes in the granule cell layer (GCL), and fibrous astrocytes in the white matter (WM). Purkinje cells (PCs) were also quantified due to their close association with BG. To assess potential dysregulation of astrocyte communication, we examined connexins, channel proteins essential in forming a functional network between astrocytes. Astrocytic connexins were visualized using single molecule in situ hybridization targeting connexin 30 (Cx30) and connexin 43 (Cx43), followed by immunolabeling for ALDH1L1. Our analysis revealed significant increases in ALDH1L1 + astrocyte densities in DS specific to the PCL compared to control individuals. Astrocytic connexins were significantly downregulated in DS, with Cx43 showing marked reductions in both PCL and GCL. Overall, our findings suggest that BG in the PCL and velate astrocytes in the GCL are particularly vulnerable in the depressive phenotype. Furthermore, this study supports previous findings in the cerebral cortex and extends astrocytic dysfunction to the cerebellum suggesting a widespread disruption of astrocyte-mediated communication across the brain in depression.

Introduction

With a global prevalence exceeding 300 million individuals, depression is a leading cause of disability and represents a significant risk factor for suicide [1]. While depression and suicide are multifactorial, [2, 3], at the cellular and molecular level, astrocytic alterations have been consistently reported, particularly in frontal-limbic brain regions [4]. Astrocytes are a heterogeneous glial cell population characterized by morphological, molecular, and functional diversity within and between distinct brain areas [5–9]. Importantly, the capacity of astrocytes to support various neuromodulatory mechanisms can be partly attributed to their high expression of connexins (Cx), the protein subunits forming hemichannels and gap junctions [10, 11]. In the mature brain, the predominant connexins expressed in astrocytes are Cx30 and Cx43, with six connexin proteins assembling into hemichannels on the cell membrane [11]. The opening of such hemichannels facilitates the release of gliotransmitters, including ATP, to support normal neuronal functions. Gap junctions are formed by two apposed hemichannels. These junctions facilitate network communication between neighboring cells by the exchange of ions, metabolites, and propagation of calcium waves, forming a functional network or syncytium [10, 11].

Postmortem studies of the cerebral cortex have consistently reported changes in astrocyte morphology, densities, and the area fraction occupied by astrocytes in depressed individuals [12–16]. Collectively, these studies suggest an overall loss of astrocytes in the grey matter across multiple cortical brain

regions, with astrocyte morphology being largely spared in depressed individuals who died by suicide (DS) [4]. Complementing such morphological studies, alterations in mRNA and protein expression levels have also been observed for the canonical astrocyte markers glial fibrillary acidic protein (GFAP) and aldehyde dehydrogenase 1 family member L1 (ALDH1L1) [17–20], as well as in the critical components of gap junction channels, Cx30 and Cx43 [18, 21–24]. Although widespread dysregulation of cerebral astrocytes has been well documented in the context of depression, less is known about the potential cellular and molecular alterations in the cerebellum.

In addition to its role in motor functions, the cerebellum is now recognized for its involvement in cognitive and emotional regulation [25, 26]; critical facets of brain activity that are disrupted in depression. Growing evidence points to possible cerebellar dysfunction in depression [27]. Functional connectivity studies highlight altered connectivity between posterior lobules of the cerebellum and key cortical regions implicated in depression, including the dorsolateral prefrontal cortex, the ventromedial prefrontal cortex, and the anterior cingulate cortex, suggesting possible dysfunction of cerebellarcerebral circuits in depression [28-30]. Few postmortem studies have focused on cerebellar astrocyterelated alterations in depression. While decreases in GFAP protein levels were reported in the lateral cerebellum of depressed individuals [31], no such differences in GFAP expression levels and protein levels were observed in DS [17]. Interestingly, decreases in Cx43 expression accompanied by increases in Cx30 expression in the cerebellar cortex have been reported in DS, suggesting distinct patterns of Cx expression in this brain region [23]. To build upon this knowledge, the objective of the current study was to perform a detailed postmortem examination of cerebellar astrocytes and Purkinje cells (PCs) in neurologically and psychiatrically healthy individuals (CTRL) compared to depressed individuals who died by suicide (DS). We targeted crus I, a posterior lobule associated with cognition [25], as cognitive impairments are well documented in depression [3, 32]. Using stereological approaches, ALDH1L1 + and GFAP + astrocytes were quantified while fluorescence in situ hybridization (RNAscope) allowed us to quantify Cx43 and Cx30 in cerebellar layers. Our analysis revealed significant increases in ALDH1L1 + astrocyte densities in DS that were specific to the Purkinje cell layer (PCL). Astrocyte connexins were significantly downregulated in DS, with Cx43 showing marked reductions in both the PCL and the granule cell layer (GCL).

Methods

Postmortem cerebellar samples

Postmortem human cerebellar samples from DS and CTRL were provided by the Douglas-Bell Canada Brain Bank (https://douglasbrainbank.ca). In close collaboration with the Quebec Coroner's office, phenotypic information was obtained through standardized psychological autopsies and with informed consent from the next of kin [33]. Presence or suspected presence of any neurological or neurodegenerative disorder, as well as alcohol or substance abuse, based on clinical files and toxicology reports constituted exclusion criteria. Proxy-based interviews with one or more informants best acquainted with the donor were supplemented with information from the Coroner's report and medical

records. Toxicological analysis and information on prescriptions were also obtained. Clinical vignettes were then produced and assessed by a panel of clinicians, using Diagnostic and Statistical Manual of Mental Disorders (DSM-IV) diagnostic criteria, to establish a diagnosis [33, 34].

Tissue Dissections

Expert brain bank staff dissected cerebellar crus I from sagittal slabs with the guidance of a human brain atlas [35, 36]. 1cm³ tissue blocks containing crus I were dissected at the level of the dentate nucleus, X = 20, following the atlas of Schmahmann et al., 2000 [36]. Formalin-fixed tissue blocks were used for stereology which included 21 CTRL and 20 DS (see **Table 1** for subject characteristics) while fresh-frozen tissues from a subset of the same subjects were used for fluorescence in situ hybridization (FISH), RNAscope (16 CTRL, 18 DS, see **Table 2** for subject characteristics).

Immunolabeling

Immunolabeling was performed as previously described [37]. Briefly, 1cm³ formalin-fixed blocks were suspended in a 30% sucrose solution until equilibrium was reached followed by flash freezing in -35°C isopentane. Tissue blocks were then systematically and exhaustively sectioned into 30 µm-thick sagittal sections, mounted on Superfrost Plus glass slides, and stored at -80°C until immunostaining. Section sampling followed systematic and random sampling principles of stereology [38, 39]. Six equally spaced series of sections were immunolabelled (1200 µm between sections). Upon removal from - 80°C, sections were acclimatized to room temperature (RT) and heated in a 60°C oven for 30 min to increase section adherence to the glass slides. Sections were cooled for 5 min at RT followed by rinsing in PBS for 5 min. Antigen retrieval was performed using proteinase K (1:1000) for 15 min followed by PBS washes. To prevent non-specific binding of antibodies, sections were blocked in a solution containing 10% normal donkey serum in PBS, (NDS, Jackson ImmunoResearch Labs, Cat# 017-000-121, RRID:AB_2337258) for 1 h at RT followed by overnight incubation of primary antibodies in the same blocking solution at 4°C (chicken anti-GFAP, 1:1,000, Abcam, Cat# ab4674, RRID: AB_304558; mouse anti-ALDH1L1, 1:250, Millipore, Cat# MABN495, RRID:AB_2687399). Sections were then rinsed in PBS followed by application of secondary antibodies in blocking solution for 1 h at RT (Alexa Fluor® 488conjugated donkey anti-chicken, 1:500, Jackson ImmunoResearch labs, Cat# 703-545-155, RRID: AB_2340375; Alexa Fluor® 647-conjugated donkey anti-mouse, 1:500, Jackson ImmunoResearch Labs, Cat# 715-605-151, RRID: AB_2340863). Sections were washed in PBS and guenched for autofluorescence using TrueBlack® (Biotium, 23007) for 75 sec, then rinsed and coverslipped with Vectashield Vibrance mounting medium containing DAPI (Vector, H-1800).

Fluorescence in situ hybridization

Frozen cerebellar crus I tissue blocks were cut serially with a cryostat and 10 µm-thick sections were collected on Superfrost Plus charged slides. Fluorescence in situ hybridization was performed using Advanced Cell Diagnostics RNAscope® probes and reagents following the manufacturer's instructions. Briefly, sections were fixed in cold 10% neutral buffered formalin for 15 min, dehydrated in a series of increasing ethanol gradients (70%, 95%, 2 x 100%) and air dried for 5 min. Endogenous peroxidase activity was guenched with hydrogen peroxide for 10 min followed by PBS rinses. The following probes were then hybridized for 2 h at 40°C in a humidity-controlled hybridization oven: Hs-GJA1 (Cx43) catalogue # 444281-C1) and Hs-GJB6 (Cx30 catalogue # 541391-C3). Sections were washed twice with RNAscope wash buffer and stored in 5xSSC buffer overnight at RT. The following day, sections were rinsed twice with RNAscope wash buffer. Amplifiers were then added using the proprietary AMP reagents and the signal visualized through probe-specific HRP-based detection by tyramide signal amplification (TSA) with Opal dyes (Opal 570 for Cx30, or Opal 690 for Cx 43; Akoya Biosciences) diluted at 1:300. Immediately following the in situ hybridization protocol, immunofluorescence labelling of ALDH1L1 was performed. Sections were washed in PBS, blocked in 10% normal donkey serum, (NDS, Jackson ImmunoResearch Labs, Cat# 017-000-121, RRID:AB_2337258) for 1h at RT and incubated overnight at 4°C in 10% NDS + PBS with mouse anti-ALDH1L1 (1:250, Millipore, Cat# MABN495, RRID:AB_2687399). Following the primary antibody incubation, sections were rinsed in PBS followed by application of a secondary antibody, Alexa Fluor® 488-conjugated donkey anti-mouse (1:500, Jackson ImmunoResearch Labs, Cat# 715-545-151) for 1 hour at RT. Following PBS washes, sections were quenched for autofluorescence using TrueBlack® (Biotium, 23007) for 90 seconds, rinsed and coverslipped with Vectashield Vibrance mounting medium containing DAPI (Vector, H-1800).

Image Analysis

Immunofluorescence and Stereology. Unbiased stereology was performed using the software StereoInvestigator (MBF Bioscience, RRID:SCR_004314, United States, Stereo Investigator, RRID:SCR_002526) following previous parameters [37]. Briefly, image stacks were acquired throughout the mounted tissue thickness using a Zeiss ApoTome2 Axio Imager.M2 microscope system at 63X (N.A. 1.4). To account for wavy tissue and ensure optimal image quality, tissue thicknesses were measured at every sampling site. The optical fractionator probe was applied to the image stacks using a 9µm dissector height with 1µm guard zones. Unbiased estimates of ALDH1L1⁺ and GFAP⁺ astrocytes were quantified in 3 layers of interest (PCL, GCL, and white matter (WM)). The molecular layer (ML) was not guantified due to the sparce presence of astrocyte cell bodies observed in this layer [37]. In total 15,699 astrocytes were counted in the PCL, 5723 astrocytes were counted in the GCL, and 6110 white matter astrocytes were counted (Fig. 1A). PCs were counted live using the optical fractionator probe in the PCL to minimize imaging times. 4075 PCs were measured in total. PC body sizes were measured using the nucleator probe (isotropic sampling, 4 rays) (Fig. 2A). The Cavalieri probe was applied on the same contours used for counting to generate volume estimates in each layer. The robustness of our stereological estimates was indicated by obtaining coefficients of error (Gunderson m = 1) < 0.10 (Supplemental Table 1).

FISH and Connexins: The open-source software FIJI was used to quantify Cx30 and Cx43 puncta [40], (RRID:SCR_002285). Image stacks (1µm distance between planes) from 2 regions of interest/subject were acquired using a Zeiss ApoTome2 Axio Imager.M2 microscope system engaging the apotome at 40X (N.A 0.95). Each region of interest encompassed the ML, PCL, GCL and WM. Focus maps were set to each imaging site to ensure optimal image quality with Cx43 acting as the focus channel. Exposure times were held constant for all sections and subjects. Sum projection composite images were created from the image stacks on which each layer was outlined. 5 ALDH1L1 + cells/layer/subject/ were also annotated where ALDH1L1 labelling was used to locate positive cells and DAPI was used to trace the nuclei. The outlined DAPI nuclei were then enlarged 0.5 µm to better encompass the full extent of the ALDH1L1 + cell body (Fig. 3A). The Find Maxima function in FIJI was used to identify Cx30 puncta (prominence = 170) and Cx43 puncta (prominence = 65) [24]. To verify the accuracy of the automated puncta identification, 10 subjects (5 CTRL, 5 DS) were manually counted yielding excellent correlations (Cx30 Pearson R = 0.9696, Cx43 Pearson R = 0.9134, Supplemental Figs. 1 & 2). Custom built scripts were applied to each image which 1) counted the number of puncta in each layer for each connexin 2) counted Cx30 and Cx43 puncta in the outlined ALDH1L1 + astrocytes, and 3) generated area measurements for each layer to report density measures. All data analyses were conducted with investigators blinded to group allocation.

Statistical Analysis

Statistical analyses and graphical representations were performed using SAS JMP Student Edition 18.2.1 (SAS Institute, Cary, NC, USA). Distributions were assessed with Shapiro–Wilk tests and by examining normal quantile plots. Data that did not meet the assumption of normality were transformed accordingly. Spearman correlations assessed the relationship between dependent variables and covariates (age, postmortem interval, refrigeration delay and pH) and were included as covariates for the significant relationships. Astrocyte densities, connexin puncta densities, and the number of connexin puncta contained within ALDH1L1 + cell bodies were analyzed using mixed-effects models with layer and group as fixed factors, followed by Tukey honest significant difference (HSD) test. One female control subject was excluded from the astrocyte density analyses as it was an extreme outlier in the normal quantile plots. There was considerable variation in Cx30 puncta counts in ALDH1L1 + astrocytes. Three subjects were identified as outliers (2 female DS and 1 male CTRL) and removed from this analysis. PC parameters were analyzed using one-way analysis of variance (ANOVA) or one-way analysis of covariance (ANCOVA) models. The significance threshold was set at 0.05.

Results

Our previous study highlighted ALDH1L1 as a suitable marker for BG cell bodies while GFAP was a robust marker for BG processes and cerebellar fibrous astrocytes in the human cerebellum [37]. Furthermore, these canonical astrocyte markers exhibited distinct distribution patterns across the cerebellar layers [37]. The current study builds upon these observations by investigating astrocyte heterogeneity in the context of depression.

Increased ALDH1L1 + astrocyte densities in the Purkinje cell layer in depressed individuals ALDH1L1 + astrocyte densities: We observed a significant group X layer interaction in ALDH1L1 + astrocyte densities, F (2, 76) = 4.2455, p = 0.0179, (Fig. 1B). Post hoc comparisons using the Tukey HSD test revealed that in the PCL, ALDH1L1 + astrocyte densities were significantly higher (13%) in the DS group compared to the CTRL group (mean difference – 18424.0, 95% CI -28979.1, -7868.9, p = 0.0011). ALDH1L1 + astrocyte densities did not differ between groups in either the GCL (p = 0.9255) or in the WM (p = 0.9638).

GFAP + astrocyte densities

We found no significant differences in GFAP + astrocyte densities between CTRL and DS groups (group X layer interaction, F (2, 76) = 0.0356, p = 0.9650; main effect of group, F (1, 38) = 0.2673, p = 0.6081) (Fig. 1C).

Depressed individuals showed an increased proportion of astrocytes expressing GFAP + in the granule cell layer

We observed differences in the proportion of astrocytes immunoreactive for ALDH1L1 and GFAP between CTRL and DS groups (Fig. 1D-F). The % of ALDH1L1 + astrocytes did not differ between groups (group X layer interaction, F (2, 76) = 0.9473, p = 0.3923; main effect of group, F (1, 38) = 2.5624, p = 0.1177) (Fig. 1D). However, we observed a group X layer interaction in the % of GFAP + astrocytes, F (2, 76) = 4.2876, p = 0.0172) in the GCL specifically, where the DS group showed a 9% increase in the proportion of GFAP + astrocytes relative to the CTRL group (mean difference – 8.6030, 95% CI -14.5357, -2.6703, p = 0.0056). The % of GFAP astrocytes did not differ between groups in either the PCL (p = 0.5998) or in the WM (p = 0.3101) (Fig. 1E). Similarly, we found a group X layer interaction in the % of double-labeled ALDH1L1 + GFAP + astrocytes, F (2, 76) = 5.7120, p = 0.0049) in the GCL, where the DS group had a higher percentage (10%) of ALDH1L1 + GFAP + astrocytes compared to the CTRL group (mean difference – 10.0543, 95% CI -15.8759, -4.2327, p = 0.0012). The % of ALDH1L1 + GFAP + astrocytes did not differ between groups in either the PCL (p = 0.6692) or in the WM (p = 0.0886) (Fig. 1F).

Purkinje cell parameters were unaffected in depressed individuals

A Spearman's correlation revealed a significant negative association between PC body size and pH, ρ -0.4267, p = 0.0094, therefore pH was included as a covariate in this analysis. We did not observe a difference in the density of PCs between CTRL and DS groups, (F (1, 39) = 1.1014, p = 0.3004) (Fig. 2B). We found no differences between CTRL and DS groups in PC body size, F (1, 33) = 2.4110, p = 0.1300 (Fig. 2C). Finally, we did not observe a difference in the number of Bergmann glia (BG) surrounding each PC between CTRL and DS groups, (F (1, 38) = 1.4558, p = 0.2351) (Fig. 2D).

Decreased astrocytic connexins in depressed individuals

Connexin 43(Cx43)

We observed a significant group X layer interaction for Cx43 puncta densities, F (3, 96) = 2.7210, p = 0.0487 (Fig. 3B). Post hoc comparisons using the Tukey HSD test revealed that Cx43 puncta densities were significantly lower in the DS group compared to the CTRL group in both the PCL (26% decrease, mean difference 0.7156, 95% CI 0.2563, 1.1749, p = 0.0033) and the GCL (36% decrease, mean difference 0.4913, 95% CI 0.0320, 0.9506, p = 0.0368). Cx43 puncta densities did not differ between groups in either the ML (p = 0.5881) or the WM (p = 0.2692). Interestingly, Cx43 puncta densities were highest in the PCL, main effect of layer, F (3, 96) = 118.6972, p < 0.0001, (ML vs PCL mean difference – 1.8998, 95% CI -2.1934, -1.6062, p < 0.0001, PCL vs GCL mean difference 1.1948, 95% CI 0.9012, 1.4884, p < 0.0001, PCL vs WM mean difference 1.7624, 95% CI 1.4688, 2.0561, p < 0.0001). We also analyzed the number of Cx43 puncta specifically within ALDH1L1 + astrocyte cell bodies. A Spearman's correlation revealed a significant negative association between Cx43 puncta counts and refrigeration delay, p -0.3867, p = 0.0262, therefore refrigeration delay was included as a covariate in this analysis. While we did not observe a group X layer interaction (F (3, 92.1) = 0.1847, p = 0.9066), a main effect of group was observed, F (1, 29.9) = 4.9960, p = 0.0330 with a 24% decrease in Cx43 puncta in ALDH1L1 + astrocytes in the DS group compared to CTRLs (Fig. 3C).

Connexin 30 (Cx30)

A log transformation was applied to Cx30 puncta densities to meet the assumption of normality. Furthermore, pH was included as a covariate, as there was a significant negative relationship between pH and Cx30 puncta densities, ρ -0.4329, p = 0.0150. We did not observe a group X layer interaction (F (3, 87) = 0.1247, p = 0.9453), however there was a significant overall effect of group, F (1, 28) = 7.2132, p = 0.0120 with a 36% decrease in Cx30 puncta density in the DS group compared to CTRLs (Fig. 3D). Differential Cx30 puncta density was also observed across cerebellar layers, with the highest densities being observed in the GCL and PCL, main effect of layer, F (3, 87) = 118.9113, p < 0.0001, (ML vs GCL mean difference – 1.5985, 95% CI -1.8597, -1.3373, p < 0.0001, GCL vs WM mean difference 1.1063, 95% CI 0.8452, 1.3675, p < 0.0001, PCL vs GCL mean difference – 0.1417, 95% CI -0.4029, 0.1195, p = 0.4900, ML vs PCL mean difference – 1.4568, 95% CI -1.7180, -1.1956, p < 0.0001, PCL vs WM mean difference 0.9647, 95% CI 0.7035, 1.2259, p < 0.0001). We next assessed the number of Cx30 puncta specifically within ALDH1L1 + astrocyte cell bodies. A square root transformation was applied to Cx30 puncta counts to address the presence of zeros and to meet the assumption of normality. We did not observe a group X layer interaction (F (3, 87) = 0.5363, p = 0.6587). A significant group effect was observed, F (1, 87) = 0.536329) = 6.6120, p = 0.0155, with a 35% decrease in Cx30 puncta in ALDH1L1 + astrocytes in the DS group compared to CTRLs (Fig. 3E). When we included sex in the model we observed a significant group X sex X layer interaction (F (3,81) = 2.9925, p = 0.0357) where in the GCL female CTRLs had significantly higher Cx30 puncta counts in ALDH1L1 + astrocytes compared to female DS (p = 0.0023), male CTRLs (p = 0.0221) and male DS (p = 0.0335). Interestingly, a significant negative correlation was observed between

ALDH1L1 + astrocyte densities and Cx30 puncta counts within these cells in the DS group, ρ -0.3990, p = 0.0050 (Supplemental Table 2).

Discussion

Postmortem studies have consistently observed astrocytic alterations in the cerebral cortex in DS; however, few have examined the cerebellum in this context. In the present study we comprehensively quantified astrocytes and PCs within cerebellar cortical layers in crus I. We observed an increase in ALDH1L1 + astrocyte densities in the PCL in DS with no change in GFAP + astrocyte densities. However, the percentages of GFAP + astrocytes and those colocalizing with ALDH1L1 + astrocytes were higher in DS, specifically in the GCL. Additionally, astrocytic connexins were downregulated in DS, with Cx43 showing marked reductions in both the PCL and the GCL. We found no evidence for alterations in the density nor size of PCs in DS in cerebellar lobule crus I.

An increase in ALDH1L1 + astrocyte densities in the PCL in DS, could indicate a shift toward a more activated or reactive state in BG. BG cell bodies lie in close proximity to PC somas, while their radial processes span the ML, allowing dynamic interactions with PC dendritic arborizations contributing to the regulation of cerebellar synaptic transmission [41, 42]. Although we did not observe changes in PC densities or soma sizes, it remains possible that the elaborate dendritic arbors of PCs could be compromised in DS resulting in a compensatory response by BG. BG abundantly express glutamate transporters, glial high-affinity glutamate transporter (GLAST, EAAT1) and to a lesser degree glutamate transporter 1 (GLT-1, EAAT2), positioning them as key regulators of glutamate clearance and in the prevention of excitotoxicity within the cerebellum [43–45]. Atrophied PC dendrites could disrupt glutamate homeostasis by impairing the synaptic integration of glutamatergic input from climbing (via the interior olive) and parallel (via granule cells) fibers, ultimately leading to reduced glutamate clearance [46]. In response, increased reactivity in BG may lead to upregulation of GLAST (EAAT1) as a compensatory response to buffer excess glutamate and prevent further neuronal damage or dysfunction. Quantifying GLAST (EAAT1) as well as cytoskeletal and structural proteins related to PCs (examples: MAP, calbindin, actin) in crus I of DS could aid toward this understanding.

In the cerebral cortex, GFAP + astrocyte densities, protein, and mRNA expression levels are commonly decreased in depression across multiple frontal-limbic brain regions [4, 47]. Such observations suggest that gliosis is unlikely a main feature in depression in the cerebral cortex. In contrast to these findings, the current study found unaltered GFAP + astrocyte densities in DS in cerebellar crus I. An increase in the proportion of GFAP + expressing astrocytes specific to the GCL was observed, however. This could indicate that in DS, a higher percentage of astrocytes are shifting toward a reactive phenotype without astrocyte proliferation or loss, suggesting subtle glial dysfunction or an early stress response without overt astrogliosis. The GCL layer specificity of this finding suggests that velate astrocytes are the primary astrocytic subtype undergoing this transition. Velate astrocytes wrap their processes around cerebellar glomeruli; areas of intense intertwined connections composed of mossy fibers rosettes, Golgi neuron boutons, and granule cells dendrites [48]. These astrocytes display low expression of AMPA

receptors GluA1 and GluA4, and the glutamate transporter, GLAST, while presenting high expression of the water channel aquaporin 4 (AQP4) [49, 50]. Their positioning and protein expression profiles suggest that velate astrocytes may regulate tissue homeostasis and cerebellar circuit functioning [51]. As such, a higher proportion of astrocytes exhibiting a reactive phenotype in DS could disrupt the expression and localization of AQP4, as is observed in the cerebral cortex in DS [14, 21] and in animal models of depression [52, 53] potentially leading to impairments in glymphatic function as well as disruptions in the blood brain barrier [54, 55].

We also assessed intercellular communication of astrocytes by quantifying two main astrocytic connexins, Cx43 (GJA1) and Cx30 (GJB6), at the RNA level across the cerebellar layers in crus I. While an overall decrease in Cx30 puncta density was observed in DS, Cx43 puncta density was explicitly reduced in the PCL and GCL in DS, implying prominent Cx43 alterations in BG and velate astrocytes respectively. Furthermore, we observed global reductions in Cx43 and Cx30 puncta counts specifically in ALDH1L1 + astrocyte cell bodies in DS. Taken together, these findings could suggest that in DS, connexin alterations are differentially localized, with astrocytic processes being particularly susceptible. Indeed, local translation of transcripts, including Cx43 (*GJA1*), has been observed in astrocytic peripheral processes allowing for rapid localized functional responses and fine-tuning of astrocyte interactions [56–58]. Thus, the observed reductions in Cx30 and Cx43 in DS, could lead to disruptions in ion homeostasis (via hemichannels) and/or dysfunction within the astrocyte syncytium (via gap junctions). It remains unclear if decreases in astrocytic connexins are due to an average reduction of hemichannels or gap junctions per process or due to less complexity of astrocytic processes in DS. It is tempting to speculate that the former occurs as a recent postmortem study from our lab found no differences in the fine morphology of vimentin immunoreactive astrocytes across multiple cortical regions [16], and animal models of depression have shown both atrophy [59, 60] and hypertrophy [61, 62] of GFAP immunoreactive processes. The observed decreases in Cx43 puncta density in BG within the PCL and velate astrocytes within the GCL in DS could have significant functional consequences. Cx43 is crucial for intercellular gap junction coupling, buffering of potassium, and glutamate clearance [11, 63]. Therefore, decreases in this critical connexin in BG could lead to a host of impairments such as reductions in gap junction coupling potentially leading to altered cerebellar plasticity, weakened buffering of glutamate potentially leading to PC excitotoxicity, and disrupted neurovascular coupling from possible Cx43 alterations in BG astrocytic endfeet. While Cx43 alterations in BG might alter synaptic function and compromise support for PCs, decreased Cx43 in velate astrocytes may be more closely associated to weakened metabolic support and dysregulation of cerebellar glomeruli, potentially leading to synaptic and homeostatic imbalance [48, 51].

Our findings align with those in the cerebral cortex where postmortem studies have consistently observed reductions in Cx43 protein, mRNA expression, area coverage and puncta size in DS [18, 21, 22]. Animal models of depression echo those of humans and further provide evidence for Cx43 as a potential therapeutic target. In chronic stress paradigms, decreases in Cx43 puncta, protein, and mRNA and often accompanied by an opening of Cx43 hemichannels resulting in overactivity and release of glutamate, ATP, and D/L-serine [64–69]. Elevated extracellular levels of these gliotransmitters may have harmful

effects, potentially triggering excitotoxicity and causing cell death in neighboring neurons [70]. Encouragingly, therapeutic strategies targeting astrocytic connexin dysfunction have yielded promising results. An early report found that treatment with either typical antidepressants or a glucocorticoid receptor antagonist reversed the observed Cx43 deficits in a chronic unpredictable stress model [64]. Recent findings have shown that blocking Cx43 hemichannels, thereby reducing their activity and glutamate buildup, is sufficient to produce antidepressant effects [67, 71]. It remains unclear in our human postmortem tissue how the observed decreases in Cx43 and Cx30 puncta could be related to hemichannel activity status. Sequencing-based approaches have the potential to reveal upregulation of hemichannel-related genes; however, they do not capture real-time functional activity.

The main limitations of this study need to be highlighted. First, the potential effects of antidepressants and anxiolytics should be considered. While difficult to dissociate in our cohort, it can be noted that there were no differences in astrocyte densities between the few CTRL individuals who had these substances at time of death (n = 4) compared to those CTRL individuals who did not (n = 17). However, we did observe a significant reduction in PC cell body size in CTRL individuals who had substances at time of death compared to CTRLs who did not (p = 0.0063 ANCOVA model with pH included). Our detailed PC analyses showed that PCs might not be particularly affected in DS in the cognitive lobule crus I. Exploring cerebellar lobules involved with emotional processing, for example vermis VIIA folium, may aid to understand if PCs are globally unaffected in depression. Furthermore, it remains unclear if PC dendritic arbors are affected in DS. While detailed quantifications would be beneficial and have been studied in postmortem human tissue, it remains technically challenging [72]. Along similar lines, it would be valuable to quantify astrocyte processes, particularly in BG and velate astrocytes in DS, to determine whether the observed reductions in cerebellar astrocytic connexins are indeed due to an overall decrease in hemichannels or gap junctions, as speculated. Furthermore, studies targeting oligodendrocyte-specific connexins (Cx32 and Cx47) could aid in determining if heterotypic coupling is impaired in the cerebellum in DS, as reported previously in the cerebral cortex [24].

Conclusions

Overall, the current study provides evidence for cerebellar astrocytic alterations in DS within crus I, a cerebellar lobule associated with cognitive functions. Our detailed analysis revealed that these alterations occur primarily in BG within the PCL and velate astrocytes within the GCL. Such results could suggest potential impairments in synaptic regulation and glutamate clearance mediated by BG, as well as possible disruptions in synaptic and ionic homeostasis maintained by velate astrocytes. Furthermore, this study extends the observed alterations in connexin expression from the cerebral cortex to the cerebellum, suggesting a broader disruption of astrocyte-mediated communication throughout the brain in depression.

Declarations

Data Sharing Statement All data generated for this study are contained within the manuscript. For further queries, the corresponding author NM may be contacted.

Acknowledgements We wish to express our heartfelt gratitude to the families of the donors who graciously agreed to donate the brains of their beloved family members. We also wish to thank Dominique Mirault and Vanessa Larivière for their skillful technical assistance with brain dissections. We thank Dr. Alanna J. Watt and Dr. Keith K Murai for their constructive guidance throughout this study. The present study used the services of the Molecular and Cellular Microscopy Platform at the Douglas Hospital Research Centre, and we thank Dr. Bita Khadivjam for her imaging expertise.

Funding This work was supported by a Natural Sciences and Engineering Research Council of Canada Discovery Grant (grant RGPIN-2018-05203) and a CIHR Project Grant to NM. CH received a doctoral scholarship from the Fonds de recherche en Santé – Québec (FRQ-S https://doi.org/10.69777/300756). The Douglas-Bell Canada Brain Bank is funded by platform support grants to GT and NM from the FRQ-S, Healthy Brains, Health Lives (CFREF) and Brain Canada.

Author Information

Authors and Affiliations

McGill Group for Suicide Studies, Douglas Mental Health University Institute, McGill University, Montreal, Quebec, Canada.

Christa Hercher, Gina Abajian, Maria Antonietta Davoli, Gustavo Turecki, Naguib Mechawar

Integrated Program in Neuroscience, McGill University, Montreal, Quebec, Canada.

Christa Hercher, Naguib Mechawar

Department of Psychiatry, McGill University, Montreal, Quebec, Canada.

Gustavo Turecki, Naguib Mechawar

Contributions

Conceived and designed the study: CH, NM. Investigation: CH, GA. Resources: MAD, GT, NM. Data acquisition: CH, GA. Data analysis: CH. Visualization: CH. Manuscript draft: CH, NM. Manuscript review and editing: CH, GA, MAD, GT, NM. Funding acquisition: CH, NM. Supervision: NM.

Corresponding author

Correspondence to Naguib Mechawar.

Ethics declarations

Competing interests

The authors declared no potential conflicts of interest with respect to the research, authorship, and/or publication of this article.

Ethics approval and consent to participate

The postmortem human cerebellar samples used in this study were provided by the

Douglas-Bell Canada Brain Bank (https://douglasbrainbank.ca). Written informed consent for this study was not required from the participants or the participants' legal guardians/next of kin in accordance with the local legislation and institutional requirements. The study was conducted in accordance with the local legislation and institutional requirements.

References

- 1. World Health Organization. world health organization fact sheets 2025. https://www.who.int/news-room/fact-sheets/detail/depression
- 2. Turecki G, Brent DA. Suicide and suicidal behaviour. Lancet (London, England). 2016;387(10024):1227-39. doi: 10.1016/s0140-6736(15)00234-2.
- 3. Mann JJ, Rizk MM. A Brain-Centric Model of Suicidal Behavior. Am J Psychiatry. 2020;177(10):902-16. doi: 10.1176/appi.ajp.2020.20081224.
- 4. O'Leary LA, Mechawar N. Implication of cerebral astrocytes in major depression: A review of fine neuroanatomical evidence in humans. Glia. 2021;69(9):2077-99. doi: 10.1002/glia.23994.
- 5. Bayraktar OA, Bartels T, Holmqvist S, Kleshchevnikov V, Martirosyan A, Polioudakis D, et al. Astrocyte layers in the mammalian cerebral cortex revealed by a single-cell in situ transcriptomic map. Nat Neurosci. 2020;23(4):500-9. doi: 10.1038/s41593-020-0602-1.
- 6. Endo F, Kasai A, Soto JS, Yu X, Qu Z, Hashimoto H, et al. Molecular basis of astrocyte diversity and morphology across the CNS in health and disease. Science. 2022; 378(6619):eadc9020. doi: 10.1126/science.adc9020.
- 7. Karpf J, Unichenko P, Chalmers N, Beyer F, Wittmann MT, Schneider J, et al. Dentate gyrus astrocytes exhibit layer-specific molecular, morphological and physiological features. Nat Neurosci. 2022;25(12):1626-38. doi: 10.1038/s41593-022-01192-5.
- 8. Viana JF, Machado JL, Abreu DS, Veiga A, Barsanti S, Tavares G, et al. Astrocyte structural heterogeneity in the mouse hippocampus. Glia. 2023;71(7):1667-82. doi: 10.1002/glia.24362.
- 9. Kwon W, Williamson MR, Deneen B. A functional perspective on astrocyte heterogeneity. Trends Neurosci. 2025. doi: 10.1016/j.tins.2025.06.009.
- 10. Rouach N, Avignone E, Meme W, Koulakoff A, Venance L, Blomstrand F, et al. Gap junctions and connexin expression in the normal and pathological central nervous system. Biol Cell. 2002;94(7-8):457-75. doi: 10.1016/s0248-4900(02)00016-3.

- 11. Mazaud D, Capano A, Rouach N. The many ways astroglial connexins regulate neurotransmission and behavior. Glia. 2021;69(11):2527-45. doi: 10.1002/glia.24040.
- 12. Miguel-Hidalgo JJ, Baucom C, Dilley G, Overholser JC, Meltzer HY, Stockmeier CA, et al. Glial fibrillary acidic protein immunoreactivity in the prefrontal cortex distinguishes younger from older adults in major depressive disorder. Biological psychiatry, 2000; 48(8), 861–873. https://doi.org/10.1016/s0006-3223(00)00999-9
- 13. Torres-Platas SG, Hercher C, Davoli MA, Maussion G, Labonte B, Turecki G, et al. Astrocytic hypertrophy in anterior cingulate white matter of depressed suicides. Neuropsychopharmacology. 2011;36(13):2650-8. doi: 10.1038/npp.2011.154.
- 14. Rajkowska G, Hughes J, Stockmeier CA, Javier Miguel-Hidalgo J, Maciag D. Coverage of blood vessels by astrocytic endfeet is reduced in major depressive disorder. Biol Psychiatry. 2013;73(7):613-21. doi: 10.1016/j.biopsych.2012.09.024.
- 15. Rajkowska G, Legutko B, Moulana M, Syed M, Romero DG, Stockmeier CA, et al. Astrocyte pathology in the ventral prefrontal white matter in depression. J Psychiatr Res. 2018;102:150-8. doi: 10.1016/j.jpsychires.2018.04.005.
- 16. O'Leary LA, Belliveau C, Davoli MA, Ma JC, Tanti A, Turecki G, et al. Widespread Decrease of Cerebral Vimentin-Immunoreactive Astrocytes in Depressed Suicides. Front Psychiatry. 2021;12:640963. doi: 10.3389/fpsyt.2021.640963.
- 17. Torres-Platas SG, Nagy C, Wakid M, Turecki G, Mechawar N. Glial fibrillary acidic protein is differentially expressed across cortical and subcortical regions in healthy brains and downregulated in the thalamus and caudate nucleus of depressed suicides. Mol Psychiatry. 2016;21(4):509-15. doi: 10.1038/mp.2015.65.
- 18. Nagy C, Suderman M, Yang J, Szyf M, Mechawar N, Ernst C, et al. Astrocytic abnormalities and global DNA methylation patterns in depression and suicide. Mol Psychiatry. 2015;20(3):320-8. doi: 10.1038/mp.2014.21.
- 19. Zhang L, Verwer RWH, Zhao J, Huitinga I, Lucassen PJ, Swaab DF. Changes in glial gene expression in the prefrontal cortex in relation to major depressive disorder, suicide and psychotic features. J Affect Disord. 2021;295:893-903. doi: 10.1016/j.jad.2021.08.098.
- 20. Rahimian R, Perlman K, Fakhfouri G, Mpai R, Richard VR, Hercher C, et al. Proteomic evidence of depression-associated astrocytic dysfunction in the human male olfactory bulb. Brain Behav Immun. 2024;122:110-21. doi: 10.1016/j.bbi.2024.08.016.
- 21. Medina A, Watson SJ, Bunney W, Jr., Myers RM, Schatzberg A, Barchas J, et al. Evidence for alterations of the glial syncytial function in major depressive disorder. J Psychiatr Res. 2016;72:15-21. doi: 10.1016/j.jpsychires.2015.10.010.
- 22. Miguel-Hidalgo JJ, Wilson BA, Hussain S, Meshram A, Rajkowska G, Stockmeier CA. Reduced connexin 43 immunolabeling in the orbitofrontal cortex in alcohol dependence and depression. J Psychiatr Res. 2014;55:101-9. doi: 10.1016/j.jpsychires.2014.04.007.

- 23. Nagy C, Torres-Platas SG, Mechawar N, Turecki G. Repression of Astrocytic Connexins in Cortical and Subcortical Brain Regions and Prefrontal Enrichment of H3K9me3 in Depression and Suicide. Int J Neuropsychopharmacol. 2017;20(1):50-7. doi: 10.1093/ijnp/pyw071.
- 24. Tanti A, Lutz PE, Kim J, O'Leary L, Théroux JF, Turecki G, et al. Evidence of decreased gap junction coupling between astrocytes and oligodendrocytes in the anterior cingulate cortex of depressed suicides. Neuropsychopharmacology. 2019;44(12):2099-111. doi: 10.1038/s41386-019-0471-z.
- 25. Schmahmann JD. The cerebellum and cognition. Neurosci Lett. 2019;688:62-75. doi: 10.1016/j.neulet.2018.07.005.
- 26. Kawabata K, Bagarinao E, Watanabe H, Maesawa S, Mori D, Hara K, et al. Functional connector hubs in the cerebellum. Neuroimage. 2022;257:119263. doi: 10.1016/j.neuroimage.2022.119263.
- 27. Depping MS, Schmitgen MM, Kubera KM, Wolf RC. Cerebellar Contributions to Major Depression. Front Psychiatry. 2018;9:634. doi: 10.3389/fpsyt.2018.00634.
- 28. Ma Q, Zeng LL, Shen H, Liu L, Hu D. Altered cerebellar-cerebral resting-state functional connectivity reliably identifies major depressive disorder. Brain Res. 2013;1495:86-94. doi: 10.1016/j.brainres.2012.12.002.
- 29. Zhu DM, Yang Y, Zhang Y, Wang C, Wang Y, Zhang C, et al. Cerebellar-cerebral dynamic functional connectivity alterations in major depressive disorder. J Affect Disord. 2020;275:319-28. doi: 10.1016/j.jad.2020.06.062.
- 30. Pang J, Xu J, Chen L, Teng H, Su C, Zhang Z, et al. Family history, inflammation, and cerebellum in major depression: a combined VBM and dynamic functional connectivity study. Transl Psychiatry. 2025;15(1):188. doi: 10.1038/s41398-025-03409-0.
- 31. Fatemi SH, Laurence JA, Araghi-Niknam M, Stary JM, Schulz SC, Lee S, et al. Glial fibrillary acidic protein is reduced in cerebellum of subjects with major depression, but not schizophrenia. Schizophr Res. 2004;69(2-3):317-23. doi: 10.1016/j.schres.2003.08.014.
- 32. Rhee TG, Shim SR, Manning KJ, Tennen HA, Kaster TS, d'Andrea G, et al. Neuropsychological Assessments of Cognitive Impairment in Major Depressive Disorder: A Systematic Review and Meta-Analysis with Meta-Regression. Psychother Psychosom. 2024;93(1):8-23. doi: 10.1159/000535665.
- 33. Dumais A, Lesage AD, Lalovic A, Séguin M, Tousignant M, Chawky N, et al. Is violent method of suicide a behavioral marker of lifetime aggression? Am J Psychiatry. 2005 Jul;162(7):1375-8. doi: 10.1176/appi.ajp.162.7.1375.
- 34. Tanti A, Belliveau C, Nagy C, Maitra M, Denux F, Perlman K, et al. Child abuse associates with increased recruitment of perineuronal nets in the ventromedial prefrontal cortex: a possible implication of oligodendrocyte progenitor cells. Mol Psychiatry. 2021. doi: 10.1038/s41380-021-01372-y.
- 35. Mai JK, Voss T, Paxinos G. Atlas of the human brain. 3rd ed. Amsterdam: Elsevier/Academic Press; 2008.
- 36. Schmahmann JD. MRI atlas of the human cerebellum. San Diego: Academic Press; 2000.

- 37. Hercher C, Ellerbeck K, Toutee L, Ye X, Mpai R, Belliveau C, et al. Distribution and morphological features of astrocytes and Purkinje cells in the human cerebellum. Front Neuroanat. 2025;19:1592671. doi: 10.3389/fnana.2025.1592671.
- 38. Mouton PR. Principles and practices of unbiased stereology: an introduction for bioscientists. Baltimore: Johns Hopkins University Press; 2002.
- 39. Kreutz A, Barger N. Maximizing Explanatory Power in Stereological Data Collection: A Protocol for Reliably Integrating Optical Fractionator and Multiple Immunofluorescence Techniques. Front Neuroanat. 2018;12:73. doi: 10.3389/fnana.2018.00073.
- 40. Bankhead P, Loughrey MB, Fernández JA, Dombrowski Y, McArt DG, Dunne PD, et al. QuPath: Open source software for digital pathology image analysis. Sci Rep. 2017;7(1):16878. doi: 10.1038/s41598-017-17204-5.
- 41. Buffo A, Rossi F. Origin, lineage and function of cerebellar glia. Prog Neurobiol. 2013;109:42-63. doi: 10.1016/j.pneurobio.2013.08.001.
- 42. De Zeeuw CI, Hoogland TM. Reappraisal of Bergmann glial cells as modulators of cerebellar circuit function. Frontiers in Cellular Neuroscience. 2015;9.
- 43. Lehre KP, Danbolt NC. The number of glutamate transporter subtype molecules at glutamatergic synapses: chemical and stereological quantification in young adult rat brain. The Journal of neuroscience: the official journal of the Society for Neuroscience. 1998;18(21):8751-7.
- 44. Miyazaki T, Yamasaki M, Hashimoto K, Kohda K, Yuzaki M, Shimamoto K, et al. Glutamate transporter GLAST controls synaptic wrapping by Bergmann glia and ensures proper wiring of Purkinje cells. Proc Natl Acad Sci U S A. 2017;114(28):7438-43. doi: 10.1073/pnas.1617330114.
- 45. Rothstein JD, Martin L, Levey AI, Dykes-Hoberg M, Jin L, Wu D, et al. Localization of neuronal and glial glutamate transporters. Neuron. 1994;13(3):713-25.
- 46. Yamasaki M, Aiba A, Kano M, Watanabe M. mGluR1 signaling in cerebellar Purkinje cells: Subcellular organization and involvement in cerebellar function and disease. Neuropharmacology. 2021;194. doi: 10.1016/j.neuropharm.2021.108629.
- 47. Yamamoto M, Sakai M, Yu Z, Nakanishi M, Yoshii H. Glial Markers of Suicidal Behavior in the Human Brain-A Systematic Review of Postmortem Studies. Int J Mol Sci. 2024;25(11). doi: 10.3390/ijms25115750.
- 48. Hoogland TM, Kuhn B. Recent developments in the understanding of astrocyte function in the cerebellum in vivo. Cerebellum. 2010;9(3):264-71. doi: 10.1007/s12311-009-0139-z.
- 49. Farmer WT, Abrahamsson T, Chierzi S, Lui C, Zaelzer C, Jones EV, et al. Neurons diversify astrocytes in the adult brain through sonic hedgehog signaling. Science. 2016; 19;351(6275):849-54. doi: 10.1126/science.aab3103.
- 50. Papadopoulos MC, Verkman AS. Aquaporin water channels in the nervous system. Nat Rev Neurosci. 2013;14(4):265-77. doi: 10.1038/nrn3468.
- 51. Cerrato V. Cerebellar Astrocytes: Much More Than Passive Bystanders In Ataxia Pathophysiology. J Clin Med. 2020;9(3). doi: 10.3390/jcm9030757.

- 52. Xia M, Yang L, Sun G, Qi S, Li B. Mechanism of depression as a risk factor in the development of Alzheimer's disease: the function of AQP4 and the glymphatic system. Psychopharmacology (Berl). 2017;234(3):365-79. doi: 10.1007/s00213-016-4473-9.
- 53. Wei F, Song J, Zhang C, Lin J, Xue R, Shan LD, et al. Chronic stress impairs the aquaporin-4-mediated glymphatic transport through glucocorticoid signaling. Psychopharmacology (Berl). 2019;236(4):1367-84. doi: 10.1007/s00213-018-5147-6.
- 54. Dion-Albert L, Cadoret A, Doney E, Kaufmann FN, Dudek KA, Daigle B, et al. Vascular and blood-brain barrier-related changes underlie stress responses and resilience in female mice and depression in human tissue. Nature Communications. 2022;13(1). doi: 10.1038/s41467-021-27604-x.
- 55. Medina-Rodriguez EM, Beurel E. Blood brain barrier and inflammation in depression. Neurobiology of Disease. 2022;175. doi: 10.1016/j.nbd.2022.105926.
- 56. Boulay AC, Saubamea B, Adam N, Chasseigneaux S, Mazare N, Gilbert A, et al. Translation in astrocyte distal processes sets molecular heterogeneity at the gliovascular interface. Cell Discov. 2017;3:17005. doi: 10.1038/celldisc.2017.5.
- 57. Sakers K, Lake AM, Khazanchi R, Ouwenga R, Vasek MJ, Dani A, et al. Astrocytes locally translate transcripts in their peripheral processes. Proc Natl Acad Sci U S A. 2017;114(19):E3830-E8. doi: 10.1073/pnas.1617782114.
- 58. Mazare N, Oudart M, Cohen-Salmon M. Local translation in perisynaptic and perivascular astrocytic processes a means to ensure astrocyte molecular and functional polarity? J Cell Sci. 2021;134(2). doi: 10.1242/jcs.251629.
- 59. Codeluppi SA, Chatterjee D, Prevot TD, Bansal Y, Misquitta KA, Sibille E, et al. Chronic Stress Alters Astrocyte Morphology in Mouse Prefrontal Cortex. International Journal of Neuropsychopharmacology. 2021;24(10):842-53. doi: 10.1093/ijnp/pyab052.
- 60. Virmani G, D'Almeida P, Nandi A, Marathe S. Subfield-specific effects of chronic mild unpredictable stress on hippocampal astrocytes. Eur J Neurosci. 2021;54(5):5730-46. doi: 10.1111/ejn.15234.
- 61. Du Preez A, Onorato D, Eiben I, Musaelyan K, Egeland M, Zunszain PA, et al. Chronic stress followed by social isolation promotes depressive-like behaviour, alters microglial and astrocyte biology and reduces hippocampal neurogenesis in male mice. Brain Behav Immun. 2021;91:24-47. doi: 10.1016/j.bbi.2020.07.015.
- 62. Zhang AY, Elias E, Manners MT. Sex-dependent astrocyte reactivity: Unveiling chronic stress-induced morphological changes across multiple brain regions. Neurobiol Dis. 2024;200:106610. doi: 10.1016/j.nbd.2024.106610.
- 63. Giaume C, Naus CC, Saez JC, Leybaert L. Glial Connexins and Pannexins in the Healthy and Diseased Brain. Physiol Rev. 2021;101(1):93-145. doi: 10.1152/physrev.00043.2018.
- 64. Sun JD, Liu Y, Yuan YH, Li J, Chen NH. Gap junction dysfunction in the prefrontal cortex induces depressive-like behaviors in rats. Neuropsychopharmacology. 2012;37(5):1305-20. doi: 10.1038/npp.2011.319.

- 65. Huang D, Li C, Zhang W, Qin J, Jiang W, Hu C. Dysfunction of astrocytic connexins 30 and 43 in the medial prefrontal cortex and hippocampus mediates depressive-like behaviours. Behav Brain Res. 2019;372:111950. doi: 10.1016/j.bbr.2019.111950.
- 66. Zhang NN, Zhang Y, Wang ZZ, Chen NH. Connexin 43: insights into candidate pathological mechanisms of depression and its implications in antidepressant therapy. Acta Pharmacol Sin. 2022. doi: 10.1038/s41401-022-00861-2.
- 67. Duarte Y, Quintana-Donoso D, Moraga-Amaro R, Dinamarca I, Lemunao Y, Cardenas K, et al. The role of astrocytes in depression, its prevention, and treatment by targeting astroglial gliotransmitter release. Proc Natl Acad Sci U S A. 2024;121(46):e2307953121. doi: 10.1073/pnas.2307953121.
- 68. Murphy-Royal C, Johnston AD, Boyce AKJ, Diaz-Castro B, Institoris A, Peringod G, et al. Stress gates an astrocytic energy reservoir to impair synaptic plasticity. Nat Commun. 2020;11(1):2014. doi: 10.1038/s41467-020-15778-9.
- 69. Orellana JA, Moraga-Amaro R, Diaz-Galarce R, Rojas S, Maturana CJ, Stehberg J, et al. Restraint stress increases hemichannel activity in hippocampal glial cells and neurons. Front Cell Neurosci. 2015;9:102. doi: 10.3389/fncel.2015.00102.
- 70. Verkhratsky A, Butt A, Li B, Illes P, Zorec R, Semyanov A, et al. Astrocytes in human central nervous system diseases: a frontier for new therapies. Signal Transduct Target Ther. 2023;8(1):396. doi: 10.1038/s41392-023-01628-9.
- 71. Li H, Guo A, Salgado M, Saez JC, Lau CG. The connexin hemichannel inhibitor D4 produces rapid antidepressant-like effects in mice. J Neuroinflammation. 2023;20(1):191. doi: 10.1186/s12974-023-02873-z.
- 72. Masoli S, Sanchez-Ponce D, Vrieler N, Abu-Haya K, Lerner V, Shahar T, et al. Human Purkinje cells outperform mouse Purkinje cells in dendritic complexity and computational capacity. Commun Biol. 2024;7(1):5. doi: 10.1038/s42003-023-05689-y.

Tables

Table 4: Ouble at to fo	unnation for atorcalass.	
rable 1: Subject into	rmation for stereology	
	CTRL	DS
N	21 (11male:10female)	20 (10male:10female)
Cause of death	14 natural; 7 accidental	20 suicide
Axis 1 diagnosis	0	15 MDD; 5 DD-NOS
Age (years) (p = 0.78)	56 ± 16	55 ± 17
PMI (hours)	57 ± 27	60 ± 20
(p = 0.68)		
рН	6.23 ± 0.21 (N=19)	6.32 ± 0.36 (N=17)
(p = 0.45)		
Ref. delay (hours)	12 ± 13	16 ± 18
(p = 0.24)		
Medication	Toxicology	Toxicology
	1 = antidepressants	8 = antidepressants
	1 = benzodiazepine	3 = benzodiazepine
	1 = anxiolytic	1 = antidepressants & benzodiazepine
	1 = alcohol	1 = antihistamine
		1 = alcohol, atypical antipsychotic
		1 = carbon monoxide
	Last 3 months	Last 3 months
	1 = antidepressants	6 = antidepressants
	1 = benzodiazepine1 = benzodiazepine & cholinesterase inhibitor	6 = antidepressants & benzodiazepine
		1 = antidepressants & atypical
		antipsychotic

Date represent mean \pm standard deviation.

p values were generated by t-tests (age and PMI) or by Wilcoxon tests when the data failed the Shapiro-Wilks test for normality (pH and Ref. delay). Significance threshold set at 0.05.

DD-NOS depressive disorder not otherwise specified, MDD major depressive disorder, PMI postmortem interval, Ref. delay refrigeration delay.

Refrigeration delay = the delay between time of death and storage of the body in a cold room.

Table 2: Subject information for connexins			
	CTRL	DS	
N	16 (9male:7female)	18 (9male:9female)	
Cause of death	10 natural; 6 accidental	18 suicide	
Axis 1 diagnosis	0	13 MDD; 5 DD-NOS	
Age (years) (p = 0.63)	56 ± 17	53 ± 16	
PMI (hours)	54 ± 28	63 ± 18	
(p = 0.30)			
pH	6.25 ± 0.22 (N=15)	6.32 ± 0.37 (N=16)	
(p = 0.74)			
Ref. delay (hours)	9 ± 8 (N= 15)	17 ± 19	
(p = 0.06)			
Medication	Toxicology	Toxicology	
	1 = antidepressants	8 = antidepressants	
	1 = benzodiazepine	2 = benzodiazepine	
		1 = antidepressants & benzodiazepine	
		1 = antihistamine	
		1 = atypical antipsychotic	
		1 = carbon monoxide	
	Last 3 months	Last 3 months	
	1 = antidepressants	5 = antidepressants	
	1 = benzodiazepine	5 = antidepressants & benzodiazepine	
		1 = antidepressants & atypical antipsychotic	

Date represent mean ± standard deviation.

p values were generated by t-tests (age and PMI) or by Wilcoxon tests when the data failed the Shapiro-Wilks test for normality (pH and Ref. delay). Significance threshold set at 0.05.

DD-NOS depressive disorder not otherwise specified, MDD major depressive disorder, PMI postmortem interval, Ref. delay refrigeration delay.

Refrigeration delay = the delay between time of death and storage of the body in a cold room.

Figures

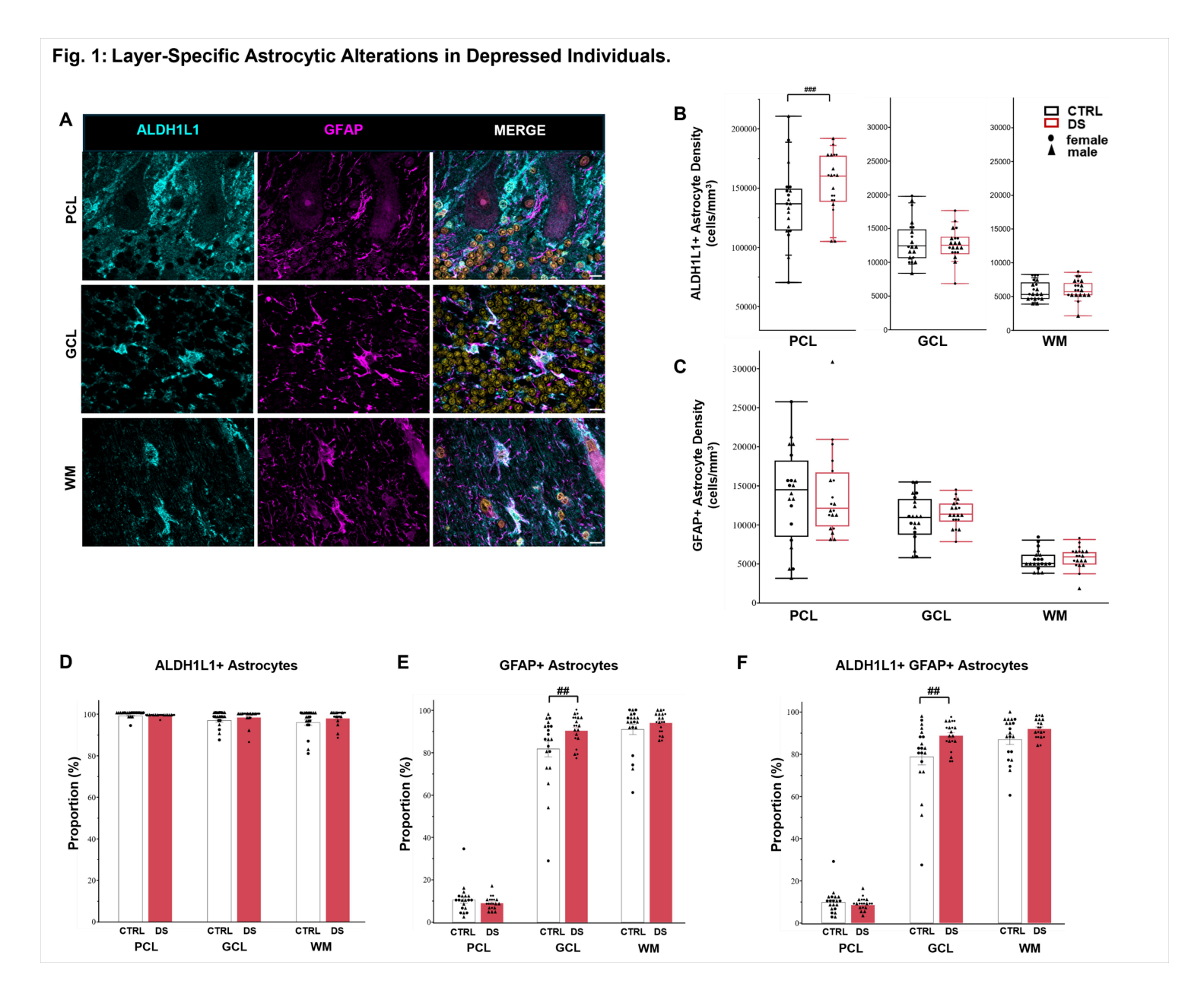


Figure 1

Quantification of cerebellar astrocytes across cerebellar layers. **A** Representative images of ALDH1L1+ (cyan) and GFAP+ (magenta) astrocytes in the cerebellar layers PCL, GCL, and WM. DAPI is shown in yellow in the merged images. Images were acquired using a Zeiss ApoTome2 Axio Imager.M2 microscope system with apotome feature engaged, 63X, scale bar $10\mu m$. **B** ALDH1L1+ astrocyte density (cells/mm³) was increased in the PCL in DS compared to CTRLs (13%, p = 0.0011). Quantile box plots

are shown. **C** No changes in GFAP+ astrocyte density (cells/mm 3) between DS and CTRL were observed. Quantile box plots are shown. **D** No differences in the proportion of ALDH1L1+ astrocytes were observed between CTRL and DS groups. Percentages are shown. **E** The proportion of GFAP+ astrocytes was higher in the GCL in the DS group (9%, p = 0.0056). Percentages are shown. **F** Similarly, the proportion of double-labeled ALDH1L1+GFAP+ astrocytes was increased in the GCL in DS compared to CTRL group (10%, p = 0.0012). Percentages are shown. Post Hoc ## p < 0.01, ### p < 0.001.

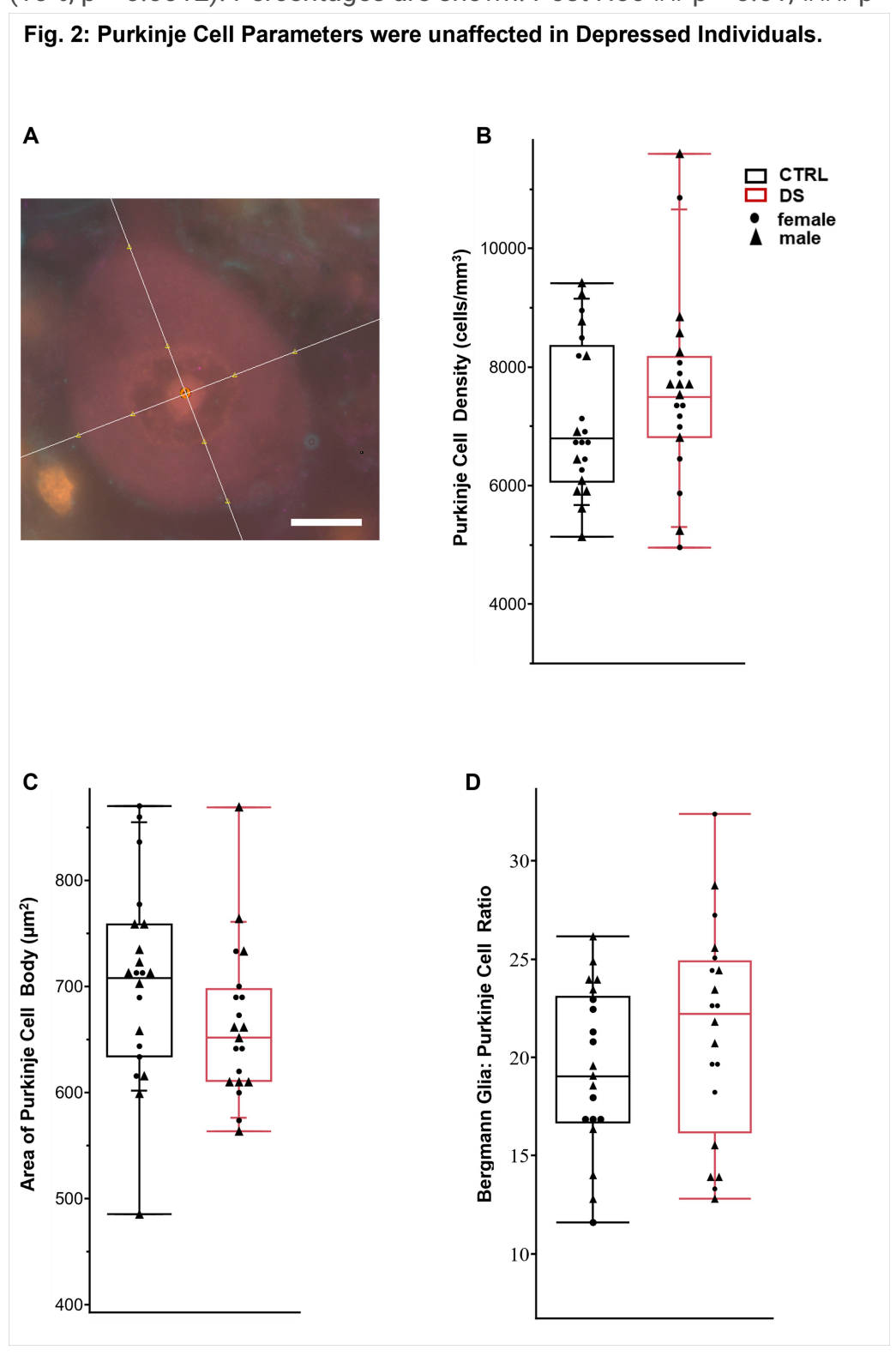


Figure 2

Purkinje cell parameters. **A** Representative image displaying the nucleator probe used to quantify PC body size. Image acquired using a Zeiss ApoTome2 Axio Imager.M2 microscope system, 63X, scale bar $10\mu m$. No differences in **B** PC density (cells/mm³), **C** PC body size (μm^2) or in **D** the number of BG surrounding one PC were observed between DS and CTRL groups. Quantile box plots are shown.

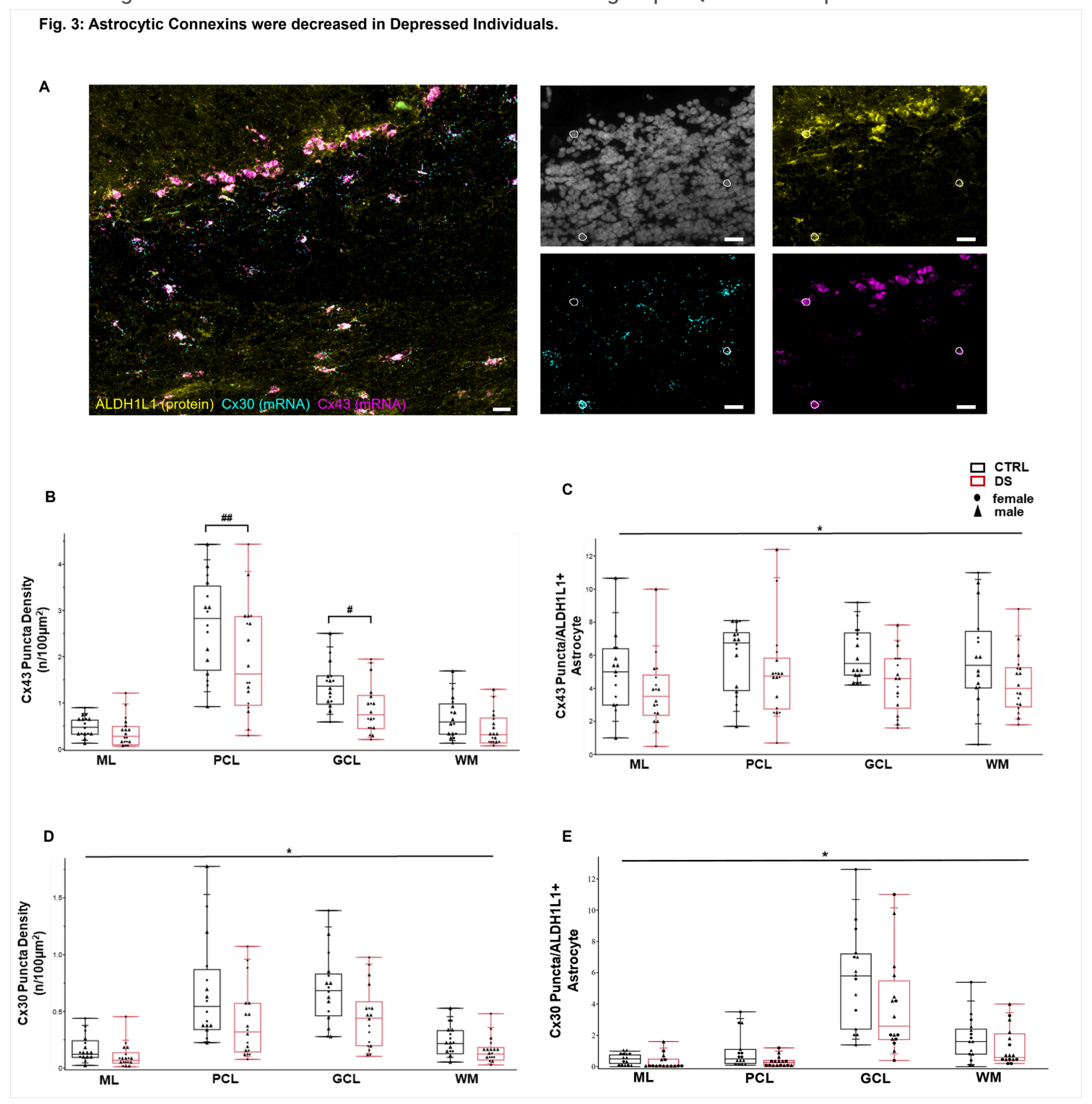


Figure 3

Quantification of connexins in the cerebellum. A Representative images displaying fluorescence in situ hybridization for Cx43 (magenta) and Cx30 (cyan) and immunolabeling for ALDH1L1 (yellow). White

circles indicate ALDH1L1+ cell bodies which were outlined guided by DAPI (grey) and enlarged. Images were acquired using a Zeiss ApoTome2 Axio Imager.M2 microscope system, apotome feature engaged, 40X, scale bar 25µm. **B** Cx43 puncta density (n/100 µm²) was decreased in the PCL (26%, p = 0.0033) and in the GCL (36%, p = 0.0368) in DS compared to CTRLs. **C** There was an overall decrease in Cx43 puncta in ALDH1L1+ astrocytes (24%, p = 0.0330) in DS compared to CTRLs. **D** There was an overall decrease in Cx30 puncta density (n/100 µm²) in DS compared to CTRLs (36%, p = 0.0120). **E** There was an overall decrease of Cx30 puncta in ALDH1L1+ astrocytes (35%, p = 0.0155) in DS compared to CTRLs. Quantile box plots are shown. * p < 0.05, Post Hoc # p < 0.05, ## p < 0.01.

Supplementary Files

This is a list of supplementary files associated with this preprint. Click to download.

- SupplementalFigure1Hercher2025TransPsych.tif
- SupplementalFigure2Hercher2025TransPsych2.tif
- SupplementalTable1.docx
- SupplementalTable2.docx